This article has been accepted for publication in IEEE Transactions on Intelligent Vehicles. This is the author's version which has not been fully edited and content may change prior to final publication. Citation information: DOI: 10.1109/TIV.2022.3156370

Ideal Reference Point in Planning and Control for Automated Car-Like Vehicles

Christoph Popp, Christoph Ziegler, Marco Sippel and Hermann Winner

***Abstract*—The choice of the reference point in automated vehicles impacts the vehicle's driving behavior. However, this influence is often not considered for planning and control tasks. To find out where the reference point should be located best, we first consider its position to be ideal if the needed lane width on the left and right side of the planned path is equal when cornering with constant curvature. For constantly curved paths we derive the ideal reference point depending on the curvature, using the kinematics of a slip angle free bicycle model. For non-stationary cornering, we analyze different maneuvers and finally, we select the reference point on the front axle. Utilizing this knowledge, the extent of a forward moving vehicle can be reduced to a point model, which does not require the orientation of the vehicle. This enables a simple and still promising approach for collision checking, where the vehicle's needed space is approximated by only one circle around the reference point. Finally, we analyze the influence of the reference point on a lateral feed-forward controller. Thus, we confirm the previously chosen reference point on the front axle for the equally distributed needed lane width and therefore recommend its use.**

***Index Terms*—Reference point, automated vehicles, bicycle model, collision check.**

I. Introduction

With the expanse of autonomous driving from the highway to urban areas, situations the automated vehicle has to deal with become more complex e. g. regarding the variety and behavior of traffic participants. As for inner city scenarios, hazardous situations have to be identified and solved in limited time and space. In order to drive autonomously, the vehicle needs to localize itself, detect the environment, predict the future behavior of other obstacles, plan its own trajectory and execute the planned strategy. All these issues need to be solved in real time on limited computational power inside the vehicle and therefore, the developed software of an autonomous vehicle needs to meet high efficiency requirements.

In order to decrease the computational effort, simplifications and approximations can be used. For example, for representing the physics of the real vehicle, either the dynamic vehicle model could be used as in [1] or a simplified kinematic vehicle model as in [2]. Both models approximate the behavior of the vehicle in different depths, whereas the dynamic model considers the tire characteristics while in the kinematic model the movement is only described by geometric equations. Another approach to save computing time is to choose representations that use mathematical simplifications.

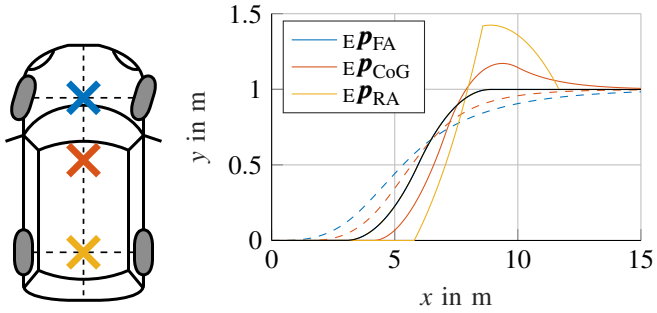

(a) (b)

Fig. 1: Common choices of the vehicle reference point ${}_{\mathrm{E}}\boldsymbol{p}_{\mathrm{ref}}$ (origin of the vehicle-fixed reference frame ${}_{\mathrm{V}}\mathscr{F}$) are the middle of the front axle ${}_{\mathrm{E}}\boldsymbol{p}_{\mathrm{FA}}$ (blue), the middle of the rear axle ${}_{\mathrm{E}}\boldsymbol{p}_{\mathrm{RA}}$ (yellow) or the center of gravity ${}_{\mathrm{E}}\boldsymbol{p}_{\mathrm{CoG}}$ (red) and are shown in (a). Even though the choice of the reference point does not change the physics of the vehicle, in a path following scenario it still influences the driven path of the vehicle. In (b), the black line represents the reference path, an S-curve, which is followed by using the above mentioned reference points. Then, the path of the middle of the front axle (solid lines) and the middle of the rear axle (dashed lines) is plotted.

A. Reference Point

With the motivation of saving computing time, we analyze the choice of the vehicle-fixed coordinate frame ${}_{\mathrm{V}}\mathscr{F}$ for planning and control tasks in the autonomous driving domain. We simplify the planning and control problem to a 2D environment in which we define ${}_{\mathrm{E}}\boldsymbol{p}$ as a 2D point in the earth-fixed coordinate system ${}_{\mathrm{E}}\mathscr{F}$. Furthermore, we use the term **reference point** ${}_{\mathrm{E}}\boldsymbol{p}_{\mathrm{ref}}$ for the origin of the vehicle-fixed coordinate frame ${}_{\mathrm{V}}\mathscr{F}$. Common choices of reference points are the middle of the front axle (**FA**), the middle of the rear axle (**RA**) or the center of gravity (**CoG**) and are shown in Fig. 1a.

Dissanayake et al. [3] use the rear axle of the vehicle as reference point for localization. By positioning an inertial measurement unit (IMU) on top of the rear axle, they use the kinematic constraints of the vehicle in this point - if the vehicle is not slipping, the lateral acceleration depends only on the centripetal force. With a different position of the IMU, the rotational acceleration of the vehicle is also measured which then needs to be taken into account in the localization algorithm.

Choosing a different reference point does not change the physics of the observed vehicle. But as shown in the localization example, there are advantages for selecting different

This work was supported by Continental AG. *(Christoph Popp and Christoph Ziegler contributed equally to this work.) (Corresponding author: Christoph Popp.)*

Christoph Popp, Marco Sippel and Hermann Winner are with the Institute of Automotive Engineering at Technical University of Darmstadt, Otto-Berndt-Straße 2, 64287 Darmstadt, Germany (e-mail: christoph.popp@tu-darmstadt.de; marco.sippel@tu-darmstadt.de; hermann.winner@tu-darmstadt.de).

Christoph Ziegler is with the Control Methods and Robotics Lab at Technical University of Darmstadt, Landgraf-Georg-Straße 4, 64283 Darmstadt, Germany (e-mail: christoph.ziegler@rmr.tu-darmstadt.de).

This article has been accepted for publication in IEEE Transactions on Intelligent Vehicles. This is the author's version which has not been fully edited and content may change prior to final publication. Citation information: DOI: 10.1109/TIV.2022.3156370

points. Since the choice of the reference point is not discussed in literature to our best knowledge, we analyze this for the tasks of planning and control. In Fig. 1b, a vehicle follows a given reference path using different reference points ${}_{\mathrm{E}}\boldsymbol{p}_{\mathrm{ref}}$. For each reference point, we determine the needed steering angles using the bicycle model introduced in Sec. II to exactly follow the reference path. The positions of the middle of the vehicle's front axle (solid lines) and its rear axle (dashed lines) along the path are calculated using geometric transformations and a spatial discretization of 0.01 m. Due to different reference points, different trajectories are driven. Selecting a reference point behind the front axle results in an overshoot of the front axle while selecting a reference point ahead smoothes the driven path. This effect is often disregarded during the planning task but should be considered, especially when using point-planning algorithms like Hybrid A* [4] or RRT* [5] where the vehicle is approximated as a point and its geometric extent is neglected. Therefore, we analyze the position of the reference point and optimize it in order to equalize the lane space needed to both sides of the planned trajectory.

Oliveira et al. [6], [7] also aim for an equalized distribution of the needed lane space by adding geometric and kinematic conditions to the motion planner with the focus on heavy-duty vehicles like buses or tractor-trailers. While the motivation for their approach is similar, Oliviera et al. add a component to the objective function of their optimization problem in order to reach equal space occupation. In our paper, we try to analytically find an ideal reference point position, which indirectly solves this problem independently of the used planning algorithm and the objective function. Like that, the complexity of the planning algorithm as well as the needed computation time are not increased.

B. Choice of Reference Point in the Literature

To the best of our knowledge there is no publication which discusses the choice of reference point for the planning task. Most of them present the position of the reference point only briefly either in text or in graphics. Therefore, in the following we discuss the positions of the reference point that were chosen in other publications.

First, all reference points are located in the lateral middle of the vehicle, to be exactly in one of the three positions presented in Fig. 1a. Here has to be noted that the position of the CoG is only an approximation because in the real vehicle it is dependent on e. g. passengers, loading and fuel level.

Planning algorithms are mostly independent of the chosen reference point and publications focus on finding a solution of a PSPACE-hard planning problem [8]. Therefore, the effect of the reference point on the driven trajectory is neglected. For example, Werling et al. [9] use ${}_{\mathrm{E}}\boldsymbol{p}_{\mathrm{CoG}}$ as reference point for their Frenet coordinate planner. Seccamonte et al. [10] use ${}_{\mathrm{E}}\boldsymbol{p}_{\mathrm{RA}}$ for their model predictive control planner to maximize the lateral clearance of the vehicle.

In contrast to the planning task, the influence of the reference point in the control task is larger. Additionally, the chosen error metric for the feedback controller impacts the result of the control task. In the survey of Paden et al. [11], three simple controllers with different reference points and error metrics for the lateral vehicle control are compared. The pure pursuit controller [12] minimizes the distance of ${}_{\mathrm{E}}\boldsymbol{p}_{\mathrm{RA}}$ to a future point on the trajectory and tracks straight paths well but has problems in curves. In [13] the lateral offset (minimal distance) of the middle of the rear axle to the path is fed back. This results in a second order response with overshooting and also works when driving backwards. In contrast, [2] feeds back the lateral offset of the middle of the front axle to the path resulting in a first order response without overshooting but is not able to drive backwards.

C. Contribution and Overview

Our contribution in this article is three-folded. First, we derive the ideal position of the reference point based on geometric reasoning. Second, we present a simple collision check which is based on our previous findings. Third, we analyze the influence of the reference point on a lateral feedforward controller.

This leads to the following structure of this paper: after the presentation of the used vehicle model in Sec. II we derive the ideal position of the reference point for curves with constant curvature κ in Sec. III. Afterwards, in Sec. IV, we analyze different reference points when the curvature of the path is non-constant. In Sec. V we present a simple collision check where we apply the previously gained knowledge about the reference point. Finally, we analyze the influence of the reference point on a lateral tracking controller in Sec. VI before we conclude the paper in Sec. VII.

II. Vehicle Model

In this work, we assume that the vehicle is rectangular in the xy-plane and has the length, width and axle positions of a car-like vehicle. Compared to the real vehicle geometry, this assumption results in overestimation of the needed lane width (**nlw**) in curves, so it is a conservative simplification that we use in our vehicle model. The nlw corresponds to the lateral space that the vehicle needs while cornering. The constant geometric parameters being used in later calculations represent our test vehicle, a Volkswagen Passat (B8), and are listed in Tab. I. Still, the geometric considerations in this work are independent of the specific geometric parameters.

To analyze the vehicle behavior depending on the chosen reference point, we apply the kinematic bicycle model with no slip angle on both axles and use the MATLAB-solver ode45 for solving the model's differential equations. According to Polack et al. [14], this kinematic model can be used for consistent motion planning when the lateral acceleration of the vehicle is limited to $0.5\mu g$. It includes the states $\boldsymbol{x} = [{}_{\mathrm{E}}x_{\mathrm{ref}}, {}_{\mathrm{E}}y_{\mathrm{ref}}, \psi]^{\mathrm{T}}$ and $\boldsymbol{u} = [v, \delta]^{\mathrm{T}}$, whereas

${}_{\mathrm{E}}x_{\mathrm{ref}}, {}_{\mathrm{E}}y_{\mathrm{ref}}$: position of the reference point,
ψ : orientation of the vehicle,
v : speed of the vehicle,
δ : front wheel steering angle.

This article has been accepted for publication in IEEE Transactions on Intelligent Vehicles. This is the author's version which has not been fully edited and content may change prior to final publication. Citation information: DOI: 10.1109/TIV.2022.3156370

TABLE I: Values of geometric parameters of the used vehicle model.

Symbol	Description	Value
l	Wheelbase	2.79 m
l_{fr}	Length from rear axle to vehicle front	3.75 m
w	Vehicle width	1.83 m

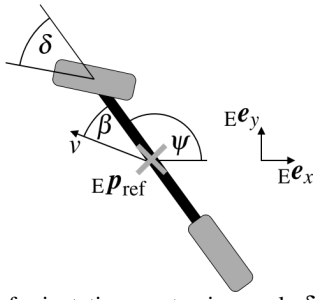

Fig. 2: Definition of orientation ψ, steering angle δ and sideslip angle β in the bicycle model.

Further parameters are

β : sideslip angle of the vehicle,

l : wheelbase,

l_{ref} : length between rear axle and reference point.

Definitions of the mentioned angles ψ, δ and β can be found in Fig. 2.

If the reference point is located in front of the rear axle, so $l_{\mathrm{ref}} > 0$, its motion is described by

$$ {}_{\mathrm{E}}\dot{x}_{\mathrm{ref}} = v\cos(\psi+\beta)\,, \tag{1} $$

$$ {}_{\mathrm{E}}\dot{y}_{\mathrm{ref}} = v\sin(\psi+\beta)\,, \tag{2} $$

$$ \dot{\psi} = \frac{v\cos\beta\tan\delta}{l} \tag{3} $$

with

$$ \beta = \arctan\left(\frac{l_{\mathrm{ref}}\tan\delta}{l}\right). \tag{4} $$

The sideslip angle β describes the direction of movement relative to the orientation of the vehicle and therefore the direction of the velocity vector. For the used kinematic model, the velocity vector starting in the reference point is always tangential to the reference path for path following. In case of $l_{\mathrm{ref}} = l$, the relationship of (4) can be simplified to $\beta = \delta$. Assuming slip angle free driving, either β or δ are required for path following. However, not all path planning approaches (e. g. A* [15] or RRT [16]) deliver information about one of these parameters along the path. That's why we derive β directly from a continuously differentiable path with the following kinematic considerations. The sideslip angle can be described by the difference between the course angle ψ_{c} and the yaw angle ψ of the vehicle. Based on this applies

$$ \frac{\mathrm{d}\beta}{\mathrm{d}s} = \frac{\mathrm{d}\psi_{\mathrm{c}}}{\mathrm{d}s} - \frac{\mathrm{d}\psi}{\mathrm{d}s} = \kappa - \frac{\mathrm{d}\psi}{\mathrm{d}s}, \tag{5} $$

whereas s is the travelled distance along the path. Using

$$ \mathrm{d}\psi = \frac{\mathrm{d}s}{R_{\mathrm{M}}} = \frac{\mathrm{d}s\cdot\sin\beta}{l_{\mathrm{ref}}} \tag{6} $$

with the distance R_{M} from the reference point to the instant center of rotation and using small-angle approximation we get

$$ \frac{\mathrm{d}\beta}{\mathrm{d}s} = \kappa - \frac{\sin\beta}{l_{\mathrm{ref}}} \approx \kappa - \frac{\beta}{l_{\mathrm{ref}}} = \frac{1}{l_{\mathrm{ref}}}(\kappa l_{\mathrm{ref}} - \beta)\,. \tag{7} $$

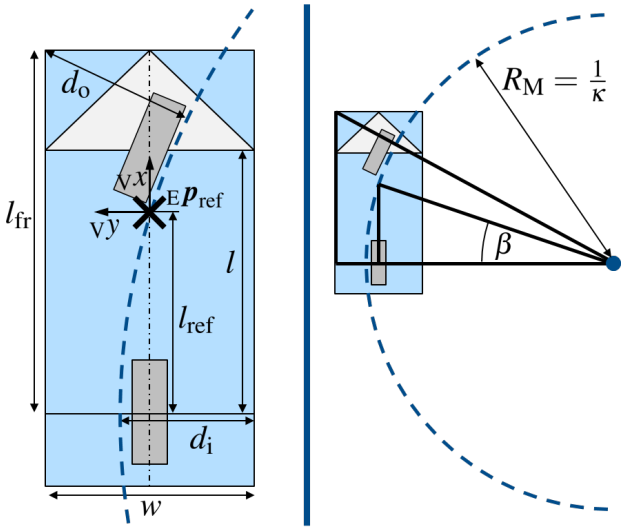

Fig. 3: The geometric parameters of the vehicle are displayed in the left part of the figure: length from rear axle to vehicle front l_{fr}, wheelbase l and body width w. The right part shows the approach to find the ideal reference point for a constant curvature κ by drawing two right-angled triangles and applying Pythagorean Theorem. Setting $d = d_i = d_o$, we get two equations with two unknowns d and l_{ref}.

This equation corresponds to a first-order lag element (also known as PT1 element) $y = \mathrm{PT1}(u,\tau)$ with input u, output y and time constant τ

$$ \frac{\mathrm{d}y}{\mathrm{d}t} = \frac{1}{\tau}(u-y)\,. \tag{8} $$

Thus, the time constant τ is a path constant l_{ref} in our case and the input signal u corresponds to κl_{ref}:

$$ \beta \approx \mathrm{PT1}(\kappa l_{\mathrm{ref}}, l_{\mathrm{ref}})\,. \tag{9} $$

With this, the sideslip angle and therefore also the steering angle (cf. (4)) can be directly determined based on the reference path. Additionally, precise estimation of the needed space is possible, e.g. for parking maneuvers. We want to add that for this estimation, it is assumed that the reference point always moves exactly along the given reference path.

III. Ideal Reference Point for Paths of Constant Curvature

We consider the choice of the reference point to be ideal for trajectory planning and tracking if the needed lane width on the left and right side of the trajectory's path is equal when cornering. Like that, simple strategies for planning and control as well as collision checks are enabled.

Fig. 3 gives an overview about the parameters used in the following calculations. The requested parameter l_{ref} is the distance from the rear axle to the position of the reference point in vehicular longitudinal direction. l_{fr} represents the length from the rear axle to the front of the vehicle, the wheelbase is described by l and the width of the vehicle equals w.

In the given example, the planned path is a right turn with constant curvature κ. As Oliveira et al. [6] already found, the rear axle is the part of the vehicle where the most space is needed on the inside of the curve. Therefore, the nlw on the inside d_{i} is given by the distance between the inner end of the

This article has been accepted for publication in IEEE Transactions on Intelligent Vehicles. This is the author's version which has not been fully edited and content may change prior to final publication. Citation information: DOI: 10.1109/TIV.2022.3156370

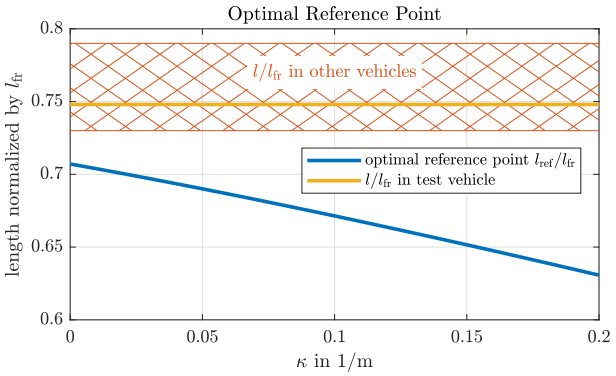

Fig. 4: The ideal position of the reference point l_{ref}/l_{fr} for $\kappa = \text{const.}$ lies between 0.63 and 0.71 depending on κ. In our test vehicle, the ideal points are 0.15 m (for $\kappa = 0\,\frac{1}{\text{m}}$) to 0.44 m (for $\kappa = 0.2\,\frac{1}{\text{m}}$) behind the front axle, which is positioned at $l/l_{fr} = 0.75$. In 37 further analyzed vehicles of various brands and vehicle classes, the front axles reach from $l/l_{fr} = 0.73$ to 0.79.

rear axle and the planned path in vehicular lateral direction or radial direction of the circular path respectively. On the outside of the bend, the front outer corner of the vehicle needs the most space [6], so the nlw to the outside d_o is given by the shortest distance between the planned path and the front outer corner of the vehicle. This distance also points in radial direction of the circular path. In order to comply with the approach described above, we define

$$d = d_i = d_o \tag{10}$$

whereas $2d$ equals the nlw.

In the right part of Fig. 3, we draw two right-angled triangles. The length of the hypotenuse of the smaller one equals the curve radius $\frac{1}{\kappa}$ and the associated catheti are described by the length l_{ref} and the distance from the center of rotation to the center of the rear axle, respectively. The hypotenuse of the second triangle equals the distance from the center of rotation to the front left corner of the vehicle and the catheti are described by l_{fr} and the distance from the center of rotation to the left end of the rear axle. Using the Pythagorean theorem, we formulate the following two equations:

$$\left(\frac{1}{\kappa}\right)^2 = l_{ref}^2 + \left(\frac{1}{\kappa} - d + \frac{w}{2}\right)^2 \tag{11}$$

$$\left(\frac{1}{\kappa} + d\right)^2 = l_{fr}^2 + \left(\frac{1}{\kappa} - d + w\right)^2. \tag{12}$$

Solving this equation system leads to

$$l_{ref}^2 = \left(\frac{l_{fr}^2}{2+\kappa w}\right)\left(1 - \frac{\kappa^2 l_{fr}^2}{4(2+\kappa w)}\right) \tag{13}$$

$$2d = \frac{2w + \kappa(w^2 + l_{fr}^2)}{2+\kappa w} \tag{14}$$

so the position of the reference point as well as the nlw depend on the curvature κ and the geometry of the vehicle. In Fig. 4, the ideal l_{ref} is set in relation to l_{fr} and plotted over κ, where $\kappa = 0.2\,\frac{1}{\text{m}}$ represents approximately the smallest feasible circular turn of the vehicle. In the used test vehicle the front axle is at $l/l_{fr} = 0.75$, so the determined ideal positions of the reference point lie slightly behind the front axle. The position of the front axle was also analyzed for 37 further

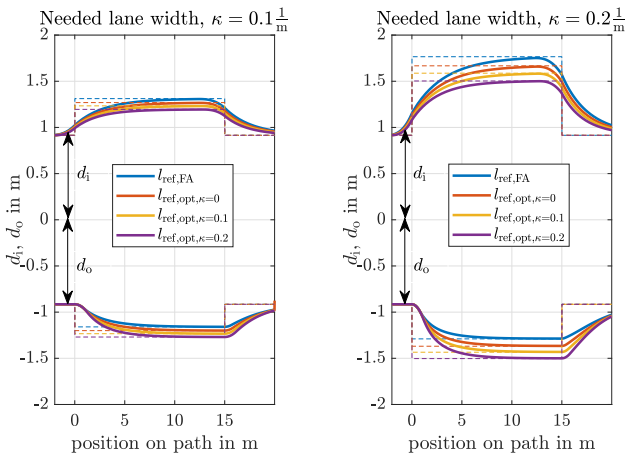

Fig. 5: Needed lane width ($d_i + d_o$) for κ jumping from zero to $0.1\,\frac{1}{\text{m}}$ in plot (a) and to $0.2\,\frac{1}{\text{m}}$ in plot (b). κ jumps back to zero after a path length of 15 m. The solid lines represent d_i and d_o for different reference points. The dashed lines show d_i and d_o in case of stationary cornering with the given κ. The choice of a non-ideal reference point has less impact on the nlw-deviations from the equal distribution to left and right for smaller κ (a) than for bigger κ (b). The assumption of stationary cornering overestimates the actual nlw after the first jump of κ until steady state is reached but also underestimates the nlw e.g. after κ returns to zero.

vehicles of various brands and vehicle classes. There, the front axle positions reach from $l/l_{fr} = 0.73$ to 0.79, so the previous statement about the ideal reference points applies for these vehicles as well.

We want to mention that the previously derived equations also apply for larger front-steered rectangular vehicles with two axles, e. g. buses, as long as the distance from the rear axle to the vehicle rear is smaller than l_{fr}. However, the exact position of the ideal reference point can vary due to the different geometric proportions. Furthermore, the range of drivable curvature is significantly reduced for vehicles with a longer wheelbase. In the following, we will only consider typical passenger vehicles like the one introduced in Tab. I.

If the reference point was defined dependent on κ, it would change its longitudinal position during driving on non-constantly curved paths. Planning and control would get even more complex, so we do not pursue the idea of a dynamic reference point any further. The goal is rather to establish one reference point that results in the smallest deviations in the nlw for various scenarios.

IV. Ideal Reference Point for Non-Stationary Cornering

In the previous section, only stationary cornering was considered. Based on this, in the following section we take a look at scenarios where the curvature is not constant.

A. Influence of non-ideal reference points

Fig. 5 shows the nlw if the reference point is chosen ideally or non-ideally. In order to compare the deviations at different curvatures, $\kappa = 0.1\,\frac{1}{\text{m}}$ and $\kappa = 0.2\,\frac{1}{\text{m}}$ are simulated for non-stationary cornering approximately up to stationary cornering.

This article has been accepted for publication in IEEE Transactions on Intelligent Vehicles. This is the author's version which has not been fully edited and content may change prior to final publication. Citation information: DOI: 10.1109/TIV.2022.3156370

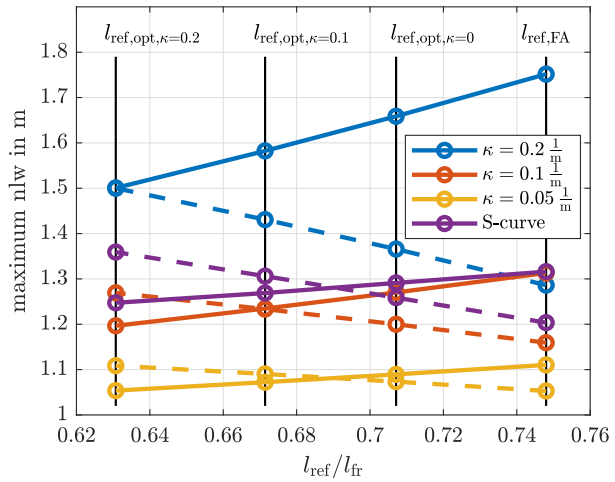

Fig. 6: Maximum nlw for different reference points. The blue, red and purple lines correspond to maneuvers of constant curvature and stationary cornering. The S-curve represented by the purple lines consists of two sections of length 3 m each, where the curvature in the first section is $\kappa = 0.2\,\frac{1}{\mathrm{m}}$ and then instantly jumps to $\kappa = -0.2\,\frac{1}{\mathrm{m}}$ for the second section. The nlw on the inside of the curve (of the first section) is represented by the solid lines, the nlw on the outside of the curve by the dashed lines.

In the left diagram, the vehicle follows a path with a curvature of $\kappa = 0.1\,\frac{1}{\mathrm{m}}$. After 15 m of constant curvature, the path goes straight, so κ jumps back to zero. Fig. 5b shows the same maneuver with $\kappa = 0.2\,\frac{1}{\mathrm{m}}$. Both scenarios are simulated with four different reference points: the ideal reference points for $\kappa = [0.2, 0.1, 0]\,\frac{1}{\mathrm{m}}$ and the reference point on the front axle. The comparison of both diagrams shows that the deviations from equally distributed nlw caused by non-ideal reference points increase with higher curvature. The influence of the choice of reference point to the deviation diminishes towards smaller curvatures, as can be seen in the maximum nlw in Fig. 6. Here, the solid lines show the nlw on the inside of the curve and the dashed lines represent the nlw on the outside of the curve. For $\kappa = 0.05\,\frac{1}{\mathrm{m}}$, the biggest difference in the nlw on the left and the right is 0.06 m and when driving straight, there would be no influence of the reference point in the nlw at all. Compared to that, non-ideal reference points at high curvatures like $\kappa = 0.2\,\frac{1}{\mathrm{m}}$ lead to highly unequally distributed nlw with differences between left and right of up to 0.48 m.

On the one hand, this is a reason to choose the reference point, which is ideal for the highest drivable curvature. On the other hand, in this case deviations would appear in every situation where the curvature is smaller than the maximum.

B. Analysis of Non-Stationary Cornering

Because the curvature often changes in real driving, we take a closer look at the actual nlw in non-stationary situations. Fig. 5 depicts the calculated nlw according to the introduced vehicle model (solid lines) and the nlw under the previous assumption of constant curvature (dashed lines). It can be seen that the assumption of κ = const. overestimates the nlw after κ jumps from zero, but also sometimes underestimates the nlw. The latter is the more critical case and appears in Fig. 5 before the curvature changes from zero and after the curvature changes to zero. The reason for underestimation of the nlw before position 0 is that the plotted lines are the inner and outer needed lane width along the reference path. If the reference point starts cornering at path position 0, the lateral position of the rear axle will be influenced even before it passes this path position, which leads to a higher nlw here.

To consider these effects, the modeling of the vehicle kinematics is required. The sideslip angle β in the bicycle model can be modeled as PT1(κl_{ref}, l_{ref}) as introduced in Sec. II at (5) to (9). The drawback of using the bicycle model to calculate the nlw is that it always needs information about the heading of the vehicle and thus requires the context of surrounding path points. It would be easier to use a point model, where each path point can be considered separately and independent of other path points, because heading is not relevant in this model. The vehicle is modeled as a circle with its center located on the reference point. To use the point model, we determine the required radius of this circle to cover the nlw.

Therefore, we examine three different maneuvers that we assume to be the most critical or curved maneuvers:

- U-turn: turn of 180° with $\kappa = 0.2\,\frac{1}{\mathrm{m}}$
- Right turn: turn of 90° with $\kappa = -0.1\,\frac{1}{\mathrm{m}}$
- S-curve: κ jumps from 0.2 to -0.2 $\frac{1}{\mathrm{m}}$, 34.4° each segment (segment length of 3 m), e.g. when the ego-vehicle is standing behind a parked vehicle and then passes it.

In previously introduced Fig. 6, the blue curves correspond to the U-turn. In this maneuver the vehicle drives an approximately stationary curve of maximum curvature and the smallest maximum nlw for both sides appears when the reference point is positioned ideally for just this $\kappa = 0.2\,\frac{1}{\mathrm{m}}$ at $l/l_{\mathrm{fr}} = 0.63$. The closer the reference point is located to the front of the vehicle, the more space is needed on the inner side of the U-turn and the less space is required on the outer side.

The right turn can also be considered as stationary cornering in the end of the maneuver. The length of this maneuver's path is 15.7 m and thus, it comes close to the scenario in Fig. 5a, where the nlw seems to reach its saturation already at about 10 m. Therefore, the red curves in Fig. 6 correspond well to the right turn maneuver. Because the curvature at the right turn is smaller than at the U-turn, the influence of the reference point is lower as well.

At the S-curve the influence of the reference point is much lower than it is at the U-turn. The biggest difference between maximum nlw on both sides for the S-curve is 0.11 m. The S-curve also needs less lateral space than the U-turn even though $|\kappa|$ is the same. The reason is that the S-curve has these big curvatures only for a short distance of 3 m and thus does not result in stationary cornering, where the maximum nlw is required for a specific κ. This can also be seen in Fig. 5b: the longer the vehicle drives along the constantly curved path, the bigger the nlw gets until it runs into saturation, which then corresponds to stationary cornering.

This article has been accepted for publication in IEEE Transactions on Intelligent Vehicles. This is the author's version which has not been fully edited and content may change prior to final publication. Citation information: DOI: 10.1109/TIV.2022.3156370

V. Collision Check

With the previously gained knowledge about the needed lane width (nlw) of a vehicle, it is possible to derive a simple collision check for car-like vehicles. With this, computational time during the planning stage can be saved. This is important, especially because a collision check needs to be done for each planning step of the planned trajectory and confiscates a substantial amount of computational resources [17], [18]. In the following, we shortly present approaches of collision checks before presenting our simplified approach.

A. Collision Checks in Literature

The problem of collision checking is originally located in the field of robotics. There, robots are often assumed to be disk-shaped like in [19], which simplifies the problem because of the disk's rotational invariance. For car-like vehicles, drawing a collision disk around the edges of the vehicle is not suitable since it would calculate a lot of false positive collisions. This may result in not finding collision-free trajectories even though they exist in reality e. g. in a narrow passage. In general, two different approaches of collision checks exist depending on the representation of the environment. Either a discrete grid map like in [20] or a geometric representation of the environment like in [21] can be used. In the following we will focus on the low-level grid-based environmental model instead of a high-level geometric representation, which requires detection and tracking of objects.

Ziegler and Stiller [20] present a fast collision check for grid-based environments by approximating the vehicle shape by three or more disks. By exploiting the commutative rule of the convolution, they first calculate a convolution of one disc with the grid-based environment before convoluting the result with different masks representing the vehicle's orientation. By precalculating the areas of collision dependent on the vehicle's orientation, they reduce the collision check to a lookup table.

Heinrich et al. [22] extend the approach from Ziegler and Stiller by only taking two circles into consideration. One is located in the front of the vehicle for outer curve collision checking whereas the second circle is located in the back for checking collisions in the inner curve. They argue, that when incrementally building a trajectory, the occupancy of the middle of the vehicle is covered by later samples of the trajectory and can therefore be omitted.

B. Simple and Fast Collision Check

For our collision check, we simplify the approach of Heinrich et al. [22]. To do so, we reduce the number of disks approximating the occupancy of the vehicle to one, which results in a point model. Instead of drawing a circle through the edges of the vehicle, we utilize the thoughts of the previous sections III and IV to choose an appropriate size of the disk. With this disk size, all needed lateral space of the whole vehicle is covered. If this disk does not collide with an object or lane marking, no part of the vehicle will neither. Further, we position the center of the disk in the reference point, because then only the position of the vehicle needs to be known and the orientation is not needed. This is especially useful when using search-based planning algorithms (e. g. A* [15], RRT [16]) where neither the orientation nor a kinematic model of the vehicle is considered. Hence, we reduce the computational effort of a collision checking algorithm by being completely rotational invariant. When using a grid map like [20], there is only need to calculate one 2D-convolution of a disk with the environment in order to calculate areas of collision. Such a convolution is shown exemplarily in Fig. 7. In the following we will discuss the position of the reference point and the size of the disk.

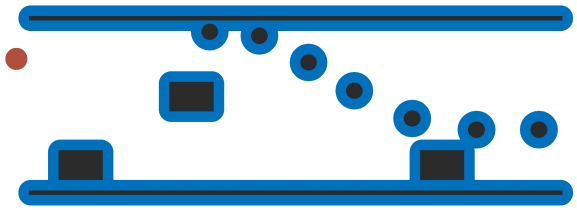

Fig. 7: Simple calculation of points of collision using a 2D-convolution. The grid map of the environment (black) was convoluted with a disk-shaped kernel (red) shown at the left side of the figure, resulting in the area of collision (blue).

If we take the ideal reference point for $\kappa = 0.2\,\frac{1}{\mathrm{m}}$ as our reference point in the previously introduced point model, the radius of the disk must be at least $r = 1.5\,\mathrm{m}$ to cover all of the presented maneuvers (cf. Fig. 6). If we put the reference point on the front axle, this radius should be at least $r = 1.76\,\mathrm{m}$. However, for our simplified approach we assume this U-turn to be irrelevant because high curvatures only appear when there is not enough space for a lower curvature path. If there is not enough space then high precision and therefore a more complex collision check is needed as well (e. g. for parking maneuvers). Thus, we neglect the blue lines in Fig. 6 and the reference point with the smallest maximum nlw is slightly behind the front axle at about $l/l_{\mathrm{fr}} = 0.735$. For reasons of simplicity, we choose the reference point exactly on the front axle, which requires the radius of the point model circle to be at least $r = 1.31\,\mathrm{m}$ (see maximum nlw for $l_{\mathrm{ref,FA}}$ in Fig. 6 neglecting the blue lines). That means that a lane width of 1.31 m on each side of the trajectory is always sufficient to pass an obstacle or a narrowing.

Another advantage of the reference point lying on the front axle is that the vehicle front is completely covered by the circle (see Fig. 8). Thus, we can use this circle easily for conservative collision checks not only in lateral direction, but also in the front of the vehicle, e. g. when stopping.

The simplifications of the approach come along with limitations which we present in the following. As the collision disk's size is larger than the actual vehicle's width (cf. Fig. 8), the approximated needed space is greater than the actual needed space. Thus, using this collision check could lead to conservative behavior in space utilization resulting in e. g. not being able to pass a narrow passage. Since the collision disk is located in the front of the vehicle, this check is only valid when driving forward. Furthermore, we assume a normal-sized car like shown in Fig. 8. If the length l_{fr} (cf. Fig. 3)

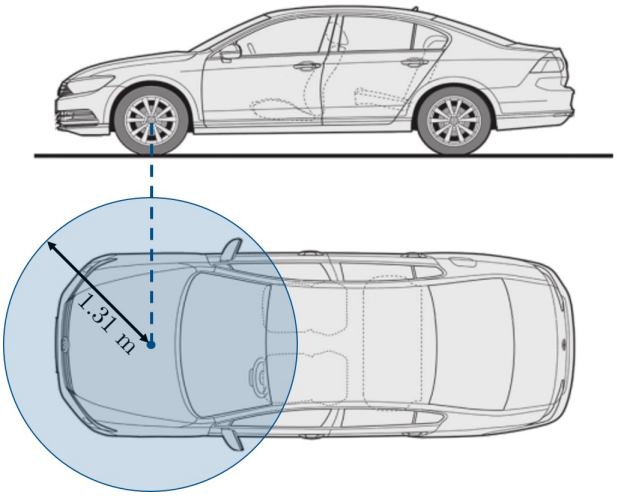

Fig. 8: Circle with $r = 1.31\,\mathrm{m}$ and its center on the front axle of VW Passat VIII (B8) (picture based on [23]). The circle covers the nlw also in curves and includes the whole vehicle front as well, which enables easy collision checks.

is too large, e. g. when considering a truck, the radius r of the collision disk gets too large in comparison to the vehicle width w and therefore, this approach doesn't make sense anymore. Additionally, the chosen disk radius limits the allowed motion of the vehicle which can be safely driven with this collision check. The maximum safe curvature is directly dependent on the disk radius (cf. (14)). Our choice of $r = 1.31\,\mathrm{m}$ results in a maximum drivable, constant curvature of $\kappa = 0.1\,\frac{1}{\mathrm{m}}$ (cf. Fig. 6). Taking non-stationary curves into account, it would also be possible to drive higher curvatures like shown with the S-curve in Fig. 6. Since it is hard to determine whether the maneuver under consideration falls outside the specified preconditions, we recommend to use a more complex approach for these situations. This is also the case if a high space utilization is a prerequisite like in automated parking. For these cases, we suggest to use an approach with higher accuracy like Heinrich et al. [22] where the position of the second disc can be calculated with the help of the sideslip angle (cf. (7)).

VI. Reference Point for Lateral Feed-Forward Control

In the previous sections, the reference point was analyzed regarding the optimization of the nlw for the planned path. In the following we examine the influence of the reference point with respect to the performance of a lateral controller. For this purpose, we implement a controller whose functionality is independent of the selected reference point. This requirement is fulfilled by the widely used controller of the Stanley robot [2], [24]–[26]. Therefore, we use this controller, whose efficacy and stability was already proven [27], as the basis for our implementation.

In this section we assume that the controller's task is the lateral control of a four wheeled vehicle which can be simplified by a bicycle model as described in Sec. II. It is also assumed that this type of controller works best with a reference point directly at ${}_{\mathrm{E}}\boldsymbol{p}_{\mathrm{FA}}$ where the controllability of the system is optimal due to the proximity to the steering axle. This assumption is evaluated in Sec. VI-B. The target to follow

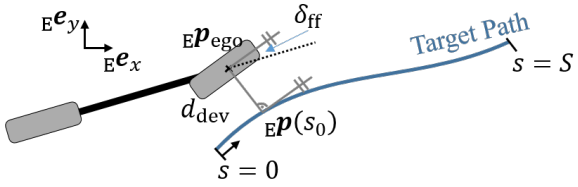

Fig. 9: Visualization of the control law, its coordinate systems and definitions.

is a path that is given by a series of points in an earth-fixed x-y-coordinate system. Each point $\boldsymbol{p}(s) = [{}_{\mathrm{E}}p_x(s), {}_{\mathrm{E}}p_y(s)]^T$ on this path is described by an x-y-position and the tangential course angle $\psi_{\mathrm{c,set}}(s)$ on to the path. The position on the path is defined by the running coordinate $s \in [0, S]$ with S being the length of the target path. The vehicle is assumed to be at the position s_0 on this path which is defined as the point with the shortest distance between the target path and the vehicle's reference point $\boldsymbol{p}_{\mathrm{ref}}$.

The main concept of the controller visualized in Fig. 9 is, that in order to follow the target path, it is necessary that the velocity vector of the vehicle points in the same direction as the tangent of the target path. When the reference point is chosen to be exactly at the front axle, this means for the idealized bicycle model that the sideslip angle equals the steering angle according to (4). Thus, the feed-forward calculates the steering angle δ_{ff} as the difference of the tangent angle $\psi_{\mathrm{c,set}}(s)$ on the path and the yaw angle ψ of the vehicle. In order to compensate the lateral deviation d_{dev}, a PD controller is used to calculate the additional steering angle δ_{PD}. The deviation d_{dev} is defined to be the shortest distance between the reference point and the target path.

Thus, the control law is described by the following time-discrete equations:

$$\delta(t_i) = \underbrace{\psi_{\mathrm{c,set}}(s_0(t_i)) - \psi(t_i)}_{\text{feed-forward } \delta_{\mathrm{ff}}} + \underbrace{\left(k_{\mathrm{p}} d_{\mathrm{dev}}(t_i) + k_{\mathrm{d}} \frac{\Delta d_{\mathrm{dev}}}{\Delta t}\right)}_{\text{control law } \delta_{\mathrm{PD}}} \tag{15}$$

$$\Delta d_{\mathrm{dev}} = d_{\mathrm{dev}}(t_i) - d_{\mathrm{dev}}(t_{i-1}) \tag{16}$$

$$\Delta t = t_i - t_{i-1} \tag{17}$$

with $d_{\mathrm{dev}}(t_i)$ being the current deviation, $d_{\mathrm{dev}}(t_{i-1})$ the deviation at the last calculation time, k_{p} the controller's gain and k_{d} the dampening coefficient. Since the feed-forward for δ is designed to work for a reference point at ${}_{\mathrm{E}}\boldsymbol{p}_{\mathrm{FA}}$, for other reference points it needs to be scaled according to the bicycle model's geometry to

$$\delta_{l_{\mathrm{ref}}} = \delta \frac{\operatorname{atan}(\kappa l)}{\operatorname{atan}(\kappa l_{\mathrm{ref}})}. \tag{18}$$

Additionally to the steering angle for reference points other than ${}_{\mathrm{E}}\boldsymbol{p}_{\mathrm{FA}}$, the target path is adapted according to the kinematics of the bicycle model in (1)-(4) to ensure that the target movement of the vehicle is identical for every reference point. This modified path $\mathcal{P}(l_{\mathrm{ref}})$ is also used as basis for the calculation of the control deviation d_{dev} and the feed-forward.

At this point it needs to be pointed out, even if the presented controller has weaknesses, as shown in [28], it was selected because the chosen reference point plays a crucial role. The

This article has been accepted for publication in IEEE Transactions on Intelligent Vehicles. This is the author's version which has not been fully edited and content may change prior to final publication. Citation information: DOI: 10.1109/TIV.2022.3156370

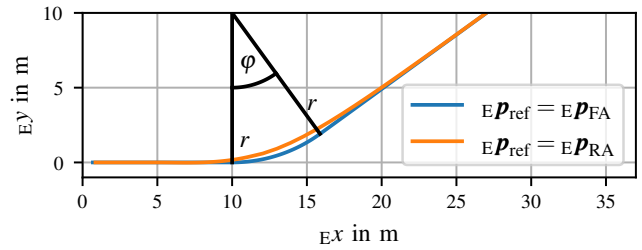

Fig. 10: Exemplary visualization of one excitation for testing the feed-forward. Path in x-y-coordinates for two different reference points and the geometry defining parameters radius r and arc-length of the curved part of the curve $\varphi = \frac{1}{4}\pi$ in radians.

singular performance of the controller was not considered in the selection, as it is not relevant to the issue under consideration. In the following subsection we first introduce our test methods and second analyze the control law with respect to the reference point. The quality of the controller is assessed on the basis of an averaged lateral deviation.

A. Test method

In order to test the performance of the control law (15), the controller was implemented in Python for the high-fidelity car simulation IPG-CarMaker 7. There, an empty scenario was generated in which the vehicle is able to drive freely. The controller itself runs on the same computer, is connected via the UDP protocol and can steer the car and control its speed. Thus the simulation in IPG-CarMaker is slowed down to work as a soft real-time simulation. For all tests, the generic simulink model from CarMaker was used. The only modification is the added UDP connectivity and a rate limiter to the steering wheel angle δ to limit the steering wheel speed to 2π per second. The used car parameter set is the IPG-CompanyCar and was not manipulated in any way. The throttle is controlled by a PID controller with the set value of a constant longitudinal speed ${}_{\mathrm{V}}v_{x,\mathrm{set}}$.

In order to compare the system behaviors for different reference points, in the following the controller is tested for different parameterized paths. The same global paths are followed by the controller for different reference points. The paths for two different reference points are visualized in Fig. 10. The path the vehicle has to follow with the reference point ${}_{\mathrm{E}}\boldsymbol{p}_{\mathrm{ref}} = {}_{\mathrm{E}}\boldsymbol{p}_{\mathrm{FA}}$ is defined by the arc length of the curved section φ, the set longitudinal speed ${}_{\mathrm{V}}v_{x,\mathrm{set}}$ and the set lateral acceleration ${}_{\mathrm{V}}a_{y,\mathrm{set}}$. The curvature κ of the arc is then approximated by the laws of circular movement to

$$\kappa = \frac{{}_{\mathrm{V}}a_{y,\mathrm{set}}}{{}_{\mathrm{V}}v_{x,\mathrm{set}}^2}. \tag{19}$$

It is assumed that the longitudinal speed of the vehicle for small sideslip angles can be set equal to the speed tangential to the target path

$$\mathcal{P}(l_{\mathrm{ref}} = l, {}_{\mathrm{V}}a_{y,\mathrm{set}}, {}_{\mathrm{V}}v_{x,\mathrm{set}}). \tag{20}$$

In order to create a solid basis for comparison, the determining parameters of the vehicle speed and the set lateral acceleration are varied. The chosen limits of the lateral acceleration are thereby determined by the physical limits of a normal passenger car to below $8\,\frac{\mathrm{m}}{\mathrm{s}^2}$. The limits of the speed are defined by an urban scenario to be below $20\,\frac{\mathrm{m}}{\mathrm{s}}$. The control parameters of the lateral controller are chosen to

$$k_p = 0.2\,\frac{\mathrm{rad}}{\mathrm{m}}, \qquad k_d = 0.1\,\frac{\mathrm{rad}\cdot\mathrm{s}}{\mathrm{m}} \tag{21}$$

in accordance with the Ziegler-Nichols tuning method. The tests were also conducted with different control parameter combinations, but yielded qualitatively equal results.

To examine the effect of the reference point on the controller, the reference point was chosen to $l_{\mathrm{ref}} \in [0.1l, 2l]$. The rearmost reference point is chosen to $l_{\mathrm{ref}} = 0.1l$, since the scaling factor from (18) is not defined for the corner case of a reference point on the rear axle. This is because a steering input has no direct influence on the lateral movement of the rear axle due to the kinematic constraints of the bicycle model. To determine the influence of a reference point that is in front of the front axle, the frontmost reference point is chosen to $l_{\mathrm{ref}} = 2l$.

B. Test results

Since we want to evaluate how well the vehicle follows the target path independent of the controller's reference point, we choose four different positions to evaluate the motion of the vehicle. These points of evaluation with $l_{\mathrm{ref,eval}}$ are equally distributed between the rear and front axle with

$$l_{\mathrm{ref,eval}} \in \left[0, \frac{l}{3}, \frac{2l}{3}, l\right]. \tag{22}$$

Furthermore, we define the error metric $\overline{d}_{\mathrm{err}}(t_i)$ as the mean value of the lateral absolute errors for these four evaluation points. The absolute lateral error for one point is defined as the shortest distance from the evaluation point to the corresponding target path. Additionally, $\overline{d}_{\mathrm{err,path}}$ is defined as the mean value of $\overline{d}_{\mathrm{err}}(t_i)$ over the whole path. In Fig. 11, $\overline{d}_{\mathrm{err,path}}$ is displayed for different reference points and target paths $\mathcal{P}(l_{\mathrm{ref}})$. The base for the comparison is the sub-figure in the middle row second column. It shows $\overline{d}_{\mathrm{err,path}}$ for a reference point of ${}_{\mathrm{E}}\boldsymbol{p}_{\mathrm{FA}}$ on the front axle. Each other sub-figure shows the difference

$$\Delta\overline{d}_{\mathrm{err,path}}({}_{\mathrm{E}}\boldsymbol{p}_{\mathrm{ref}}) = \overline{d}_{\mathrm{err,path}}({}_{\mathrm{E}}\boldsymbol{p}_{\mathrm{ref}}) - \overline{d}_{\mathrm{err,path}}({}_{\mathrm{E}}\boldsymbol{p}_{\mathrm{FA}}). \tag{23}$$

The results of this test show, that the controller reaches the best overall performance with the reference point at ${}_{\mathrm{E}}\boldsymbol{p}_{\mathrm{FA}}$. The farther back the chosen reference point lies, the worse are the results. A reference point located in front of the front axle decreases the accuracy for high speed scenarios. It also helps to increase the accuracy for the range of high lateral accelerations and low speeds. However, scenarios like this are barely performed in real driving and thus, we give less weight to this area of the diagram. Furthermore, according to [14], the consideration of other vehicle models is recommended for the planning of maneuvers above $5\,\frac{\mathrm{m}}{\mathrm{s}^2}$ lateral acceleration. For comparability, this was not done in this study, but should not be neglected when evaluating the results. This reinforces the initial assumption that the controller delivers the best performance with a reference point near the front axle. The

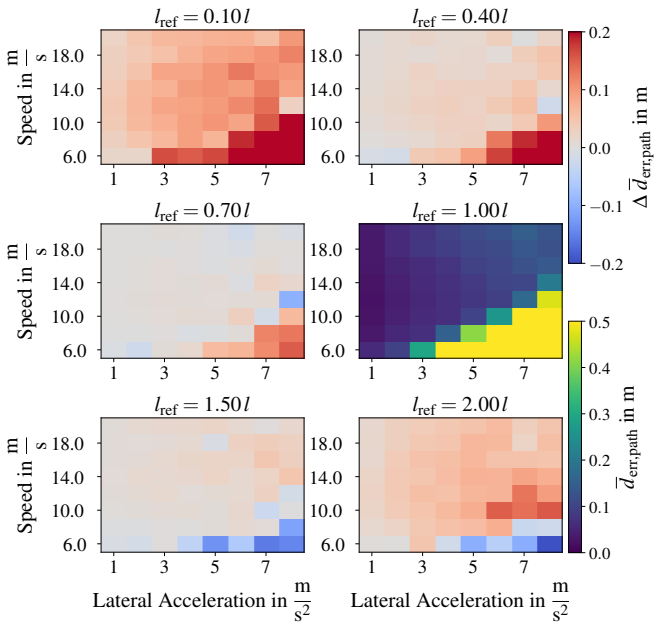

Fig. 11: $\overline{d}_{\text{err,path}}$ displayed for six different reference points and target paths $\boldsymbol{\mathcal{P}}(l_{\text{ref}})$. The base for the comparison is the sub-figure in the middle row second column. For each reference point the lateral acceleration and the speed of the vehicle are varied.

results also show that the behavior of the controlled system can be directly influenced by the choice of the reference point and thus should be considered in the development of driving controllers.

VII. Conclusion

In this article we analyzed the influence of the reference point position regarding trajectory planning and control in front-steered vehicles. For planning we defined the reference point to be ideal if the needed lane width to the left and right side of the planned trajectory is equal. By considering the geometric constraints of the bicycle model for constant curvature cornering, we presented the analytic solution to find the ideal reference point depending on the curvature of the path. In our test vehicle Passat B8 this ideal reference point is located 5-16 % of the wheelbase behind the front axle. Furthermore, our analysis of non-stationary cornering revealed on the one hand, that it is less demanding than stationary cornering regarding the needed lane width. On the other hand, we showed that there is no ideal reference point in dynamic scenarios, but considering different critical maneuvers, we conclude that a reference point on or slightly behind the front axle is a suitable choice. Additionally, this position of the reference point enables a simple and fast collision check. The simplicity results from using a point model and approximating the extent of the vehicle by only one circle. Thus, the orientation of the vehicle along the planned trajectory is not needed.

Lastly, we examined the influence of the reference point regarding the performance of a lateral feed-forward controller. The results show that the lateral deviations from the target path increase if the reference point moves from the front axle to the rear of the vehicle. Summarizing the above mentioned results, we come to the concluding recommendation to set the reference point directly on the front axle. However, we want to emphasize that the consideration of more complex vehicle models, changing road conditions and other control algorithms like e.g. model predictive control remain for future work in the field of controller related analysis.

Acknowledgment

We kindly thank Continental AG for their great cooperation within PRORETA 5, a joint research project of TU Darmstadt, University of Bremen, TU Iaşi and Continental to investigate future concepts for intelligent and learning driver assistance systems.

References

[1] C. Sun, X. Zhang, Q. Zhou, and Y. Tian, "A model predictive controller with switched tracking error for autonomous vehicle path tracking," *IEEE Access*, vol. 7, pp. 53 103–53 114, 2019.

[2] S. Thrun, M. Montemerlo, H. Dahlkamp, D. Stavens, A. Aron, J. Diebel, P. Fong, J. Gale, M. Halpenny, G. Hoffmann, K. Lau, C. Oakley, M. Palatucci, V. Pratt, P. Stang, S. Strohband, C. Dupont, L.-E. Jendrossek, C. Koelen, C. Markey, C. Rummel, J. van Niekerk, E. Jensen, P. Alessandrini, G. Bradski, B. Davies, S. Ettinger, A. Kaehler, A. Nefian, and P. Mahoney, "Stanley: The robot that won the DARPA grand challenge," *Journal of Field Robotics*, vol. 23, no. 9, pp. 661–692, 2006.

[3] G. Dissanayake, S. Sukkarieh, E. Nebot, and H. Durrant-Whyte, "The aiding of a low-cost strapdown inertial measurement unit using vehicle model constraints for land vehicle applications," *IEEE Transactions on Robotics and Automation*, vol. 17, no. 5, pp. 731–747, 2001.

[4] M. Montemerlo, J. Becker, S. Bhat, H. Dahlkamp, D. Dolgov, S. Ettinger, D. Haehnel, T. Hilden, G. Hoffmann, B. Huhnke, D. Johnston, S. Klumpp, D. Langer, A. Levandowski, J. Levinson, J. Marcil, D. Orenstein, J. Paefgen, I. Penny, A. Petrovskaya, M. Pflueger, G. Stanek, D. Stavens, A. Vogt, and S. Thrun, "Junior: The stanford entry in the urban challenge," *Journal of Field Robotics*, vol. 25, no. 9, pp. 569–597, sep 2008.

[5] S. Karaman and E. Frazzoli, "Incremental sampling-based algorithms for optimal motion planning," in *Robotics: Science and Systems VI*. Robotics: Science and Systems Foundation, jun 2010.

[6] R. Oliveira, O. Ljungqvist, P. F. Lima, and B. Wahlberg, "A geometric approach to on-road motion planning for long and multi-body heavy-duty vehicles," in *2020 IEEE Intelligent Vehicles Symposium (IV)*. IEEE, oct 2020.

[7] ——, "Optimization-based on-road path planning for articulated vehicles," *IFAC-PapersOnLine*, vol. 53, no. 2, pp. 15 572–15 579, 2020.

[8] J. H. Reif, "Complexity of the mover's problem and generalizations," in *20th Annual Symposium on Foundations of Computer Science (sfcs 1979)*. IEEE, oct 1979.

[9] M. Werling, S. Kammel, J. Ziegler, and L. Gröll, "Optimal trajectories for time-critical street scenarios using discretized terminal manifolds," *The International Journal of Robotics Research*, vol. 31, no. 3, pp. 346–359, dec 2011.

[10] F. Seccamonte, J. Kabzan, and E. Frazzoli, "On maximizing lateral clearance of an autonomous vehicle in urban environments," in *2019 IEEE Intelligent Transportation Systems Conference (ITSC)*. IEEE, oct 2019.

[11] B. Paden, M. Cap, S. Z. Yong, D. Yershov, and E. Frazzoli, "A survey of motion planning and control techniques for self-driving urban vehicles," *IEEE Transactions on Intelligent Vehicles*, vol. 1, no. 1, pp. 33–55, mar 2016.

[12] R. Wallace, A. Stentz, C. Thorpe, H. Maravec, W. Whittaker, and T. Kanade, "First results in robot road-following." in *Proceedings of the International Joint Conference on Artificial Intelligence*, 01 1985, pp. 1089–1095.

[13] C. Samson, "Time-varying feedback stabilization of car-like wheeled mobile robots," *The International Journal of Robotics Research*, vol. 12, no. 1, pp. 55–64, feb 1993.

[14] P. Polack, F. Altche, B. d'Andrea Novel, and A. de La Fortelle, "The kinematic bicycle model: A consistent model for planning feasible trajectories for autonomous vehicles?" in *2017 IEEE Intelligent Vehicles Symposium (IV)*. IEEE, jun 2017.

[15] P. Hart, N. Nilsson, and B. Raphael, "A formal basis for the heuristic determination of minimum cost paths," *IEEE Transactions on Systems Science and Cybernetics*, vol. 4, no. 2, pp. 100–107, 1968.
[16] S. M. Lavalle, "Rapidly-exploring random trees: A new tool for path planning," Tech. Rep., 1998.
[17] G. Tanzmeister, M. Friedl, D. Wollherr, and M. Buss, "Efficient evaluation of collisions and costs on grid maps for autonomous vehicle motion planning," *IEEE Transactions on Intelligent Transportation Systems*, vol. 15, no. 5, pp. 2249–2260, oct 2014.
[18] T. Stahl, A. Wischnewski, J. Betz, and M. Lienkamp, "Multilayer graph-based trajectory planning for race vehicles in dynamic scenarios," in *2019 IEEE Intelligent Transportation Systems Conference (ITSC)*. IEEE, oct 2019.
[19] Z. Qu, J. Wang, and C. Plaisted, "A new analytical solution to mobile robot trajectory generation in the presence of moving obstacles," *IEEE Transactions on Robotics*, vol. 20, no. 6, pp. 978–993, dec 2004.
[20] J. Ziegler and C. Stiller, "Fast collision checking for intelligent vehicle motion planning," in *2010 IEEE Intelligent Vehicles Symposium*. IEEE, jun 2010.
[21] A. Rizaldi, S. Sontges, and M. Althoff, "On time-memory trade-off for collision detection," in *2015 IEEE Intelligent Vehicles Symposium (IV)*. IEEE, jun 2015.
[22] B. C. Heinrich, D. Fassbender, and H.-J. Wuensche, "Faster collision checks for car-like robot motion planning," in *2018 IEEE/RSJ International Conference on Intelligent Robots and Systems (IROS)*. IEEE, oct 2018.
[23] Volkswagen, "Data sheet vw passat gte," feb 2018. [Online]. Available: https://www.motor-talk.de/forum/aktion/Attachment.html?attachmentId=767402
[24] Z. Szalay, T. Tettamanti, D. Esztergár-Kiss, I. Varga, and C. Bartolini, "Development of a test track for driverless cars: Vehicle design, track configuration, and liability considerations," *Periodica Polytechnica Transportation Engineering*, vol. 46, 03 2017.
[25] S. Dominguez, A. Ali, G. Garcia, and P. Martinet, "Comparison of lateral controllers for autonomous vehicle: Experimental results," in *2016 IEEE 19th International Conference on Intelligent Transportation Systems (ITSC)*. [S.l.]: IEEE, 11/1/2016 - 11/4/2016, pp. 1418–1423.
[26] A. A. Elmoniem, A. Osama, M. Abdelaziz, and S. A. Maged, "A path-tracking algorithm using predictive stanley lateral controller," *International Journal of Advanced Robotic Systems*, vol. 17, no. 6, p. 1729881420974852, 2020. [Online]. Available: https://doi.org/10.1177/1729881420974852
[27] G. M. Hoffmann, C. J. Tomlin, M. Montemerlo, and S. Thrun, "Autonomous automobile trajectory tracking for off-road driving: Controller design, experimental validation and racing," in *2007 American Control Conference*. IEEE, jul 2007.
[28] Z. Lu, B. Shyrokau, B. Boulkroune, S. van Aalst, and R. Happee, "Performance benchmark of state-of-the-art lateral path-following controllers," in *2018 IEEE 15th International Workshop on Advanced Motion Control (AMC)*, 2018, pp. 541–546.

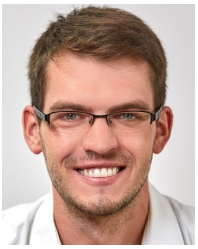

Christoph Popp received the B.S. and M.S. degrees in mechanical engineering from Technical University of Darmstadt, Germany in 2015 and 2019 respectively. There he is currently a research associate with the Institute of Automotive Engineering and working towards his Ph.D. degree. His research interests include trajectory safety and safety concepts for autonomous vehicles.

Christoph Ziegler received the B.S. and M.S. degrees in electrical engineering and information technology from Technical University of Darmstadt, Germany in 2015 and 2017 respectively. During and after his studies he worked in a startup on printing machines for printed electronics before coming back to university. Since 2019 he is a research associate with the Control Methods and Robotics Lab and working towards his Ph.D. degree. His research interests include the analysis of human driving data and trajectory planning.

Marco Sippel received the B.S. and M.S. degrees in mechanical engineering from Technical University of Darmstadt, Germany in 2013 and 2015 respectively. There he is currently a research associate with the Institute of Automotive Engineering and working towards his Ph.D. degree. His research interests include autonomous racing and vehicle behavior evaluation.

Hermann Winner studied physics at Westfälische Wilhelms-Universität in Münster/Westfalen, Germany, where he received his Ph.D. degree in 1987 as well. He began at Robert Bosch GmbH in 1987 focusing of the pre-development of "by-wire" technology and Adaptive Cruise Control (ACC). Beginning in 1995, he led the series development of ACC up to the start of production. Since 2002, he has been pursuing the research of driver assistance systems and other automotive systems engineering topics as professor at the Institute of Automotive Engineering at the Technical University of Darmstadt.